Journal of Alloys and Compounds 740 (2018) 61–67

Contents lists available at ScienceDirect

Journal of Alloys and Compounds

journal homepage: http://www.elsevier.com/locate/jalcom

Ionic conductive GeS_2-Ga_2S_3-Li_2S-LiI glass powders prepared by mechanical synthesis

Bo Fan [a], Huang Fu [b], Haiyang Li [b], Bai Xue [a, *], Xianghua Zhang [c], Zhongkuan Luo [b], Hongli Ma [c]

[a] Shenzhen Key Laboratory of Advanced Thin Films and Applications, College of Physics & Energy, Shenzhen University, Shenzhen, 518060, China
[b] Shenzhen Key Laboratory of New Lithium-ion Battery and Mesoporous Materials, College of Chemistry and Environmental Engineering, Shenzhen University, Shenzhen, 518060, China
[c] Laboratory of Glasses and Ceramics, Institute of Chemical Science, University of Rennes 1, Rennes 35042, France

ARTICLE INFO

Article history:
Received 8 October 2017
Received in revised form
29 December 2017
Accepted 30 December 2017
Available online 2 January 2018

Keywords:
Chalcogenide glass
Lithium ionic conductivity
Mechanical synthesis
Solid electrolyte

ABSTRACT

Mechanical synthesis is a low-cost industrial-compatible technique to fabricate chalcogenide glasses. In this paper, the mechanical synthesis of the ionic conductive GeS_2-Ga_2S_3-Li_2S-LiI glass powders by ball milling is studied. The structure, glass-forming ability, and ionic conductivity are compared with the reported GeS_2-Ga_2S_3-Li_2S-LiI glasses prepared by the melt-quench process. The similarity of the glass network fabricated by these two techniques is revealed by Raman spectroscopy. As for the conductivity, about 1/3–1/2 of the conductivity of the bulk glass can be achieved by simply cold-pressing the as-milled glass powders into pellets. Evident "room-temperature sintering" is observed in the Li-rich samples, which plays a key role in achieving high ionic conductivity in the cold-pressed pellets.

1. Introduction

Solid-state lithium-sulfur batteries have recently attracted increasing attention from the researchers [1,2]. With the usage of solid electrolytes as the ion-conducting medium, the problems of lithium dendrite growth and the polysulfide shuttle, which lead to safety and long-term stability issues in conventional lithium-sulfur batteries, can be avoided [3]. Moreover, a recent estimation study on the energy density demonstrated that solid-state lithium-sulfur batteries are expected to be competitive in gravimetric energy density when compared with state-of-the-art Li-ion batteries [4]. Sulfide solid electrolytes are suitable electrolytes for Li-S batteries because of their high ionic conductivity and good compatibility with the cathode materials [5–7]. The feasibility of assembling Li-S batteries with sulfide electrolytes has been demonstrated by several studies, such as using Li_2S-P_2S_5 glasses and glass-ceramics [8], argyrodite Li_6PS_5Cl [9], $Li_{9.54}Si_{1.74}P_{1.44}S_{11.7}Cl_{0.3}$ [10], Li_3PS_{4+n} [11], etc. Recently, by combining the high ionic conductivity of $Li_{10}GeP_2S_{12}$ and a well-designed cathode nanostructure, Xu et al. significantly extended the cycle life of solid-state Li-S batteries and 750 cycles at 1.0 C have been achieved [12].

Ga-Ge-S glasses are of good chemical and thermal stability [13]. By the addition of lithium, this glass system can reach an ionic conductivity of approximately 10^{-4} S/cm [14]. Therefore, Ga-Ge-S-Li glasses are expected to be a relatively stable sulfide solid electrolyte. Typically, Ga-Ge-S glasses are prepared by a conventional melt-quench process, in carbon-coated sealed quartz glass tubes or in vitreous carbon crucibles sealed in quartz glass tubes [14,15]. These techniques are not quite suitable for large-scale production due to the consumption of the high-cost quartz glass tubes. Mechanical synthesis by ball milling has been demonstrated to be a quartz-glass-tube-free technique by which to prepare chalcogenide glasses [16–18]. This technique is more compatible with industrial production. Moreover, the glasses prepared by mechanical synthesis possess similar structure and properties as those prepared by the melt-quench process [18]. In this paper, ball milling is applied to mechanically synthesize GeS_2-Ga_2S_3-Li_2S-LiI glasses. The structure and ionic conductive properties are studied and compared with the reported GeS_2-Ga_2S_3-Li_2S-LiI glasses prepared by the melt-quench process.

* Corresponding author.
E-mail address: baixue@szu.edu.cn (B. Xue).

https://doi.org/10.1016/j.jallcom.2017.12.356
0925-8388/

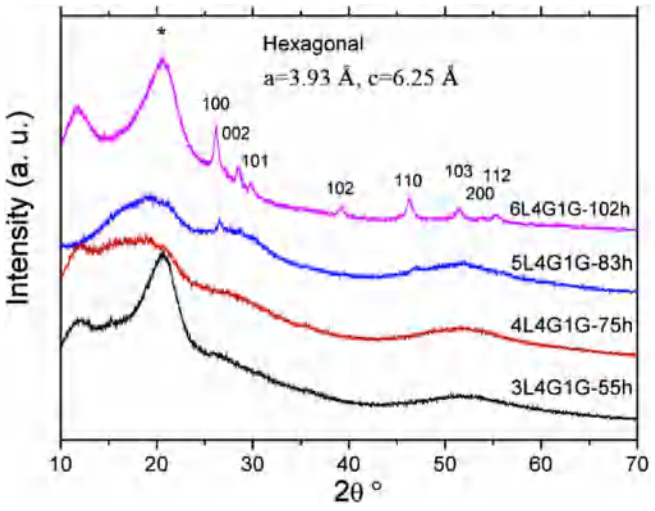

Fig. 1. XRD patterns of the GeS_2-Ga_2S_3-Li_2S glass powders in Series A, which are prepared by mechanical milling. Amorphization duration is noted in the legend. The broad peak marked by an asterisk is ascribed to a polyimide cover film.

2. Experimental procedures

GeS_2-Ga_2S_3-Li_2S-LiI glasses were prepared by the mechanical milling method. Starting materials, Ge (99,99%, Alfa Aesar), Ga (99.99%, Alfa Aesar), S (99%, Alfa Aesar), Li_2S (99.9%, Alfa Aesar), and LiI (99.9%, Alfa Aesar) were weighed according to the glass composition. Then, 8 g starting materials were put into a tungsten carbide jar with 10 tungsten carbide grinding balls (φ = 10 mm). The filling rate, namely the ratio of the volume of the balls and starting materials to the total volume of the jar, was approximately 2/3. The mechanical milling was conducted at 600 rpm using a planetary ball mill apparatus (Pulverisette 7, Fritsch GmbH, Germany). All the operations were conducted in an Ar-filled glove box. Two series of glasses were studied. Series A is only composed of GeS_2, Ga_2S_3 and Li_2S, whose composition is (100-x) ($0.8GeS_2$-$0.2Ga_2S_3$)-xLi_2S (in mol%), x = 30, 40, 50 and 60, and are denoted 3L4G1G, 4L4G1G, 5L4G1G, and 6L4G1G, respectively. Series B has the composition (50-y) ($0.8GeS_2$-$0.2Ga_2S_3$)-(50-y) Li_2S-2yLiI (in mol%), y = 10, 20, 30 and 40; that is, partially substituting Li_2S by LiI in the sample 5L4G1G. They are denoted 10I5L4G1G, 20I5L4G1G, 30I5L4G1G, and 40I5L4G1G, respectively.

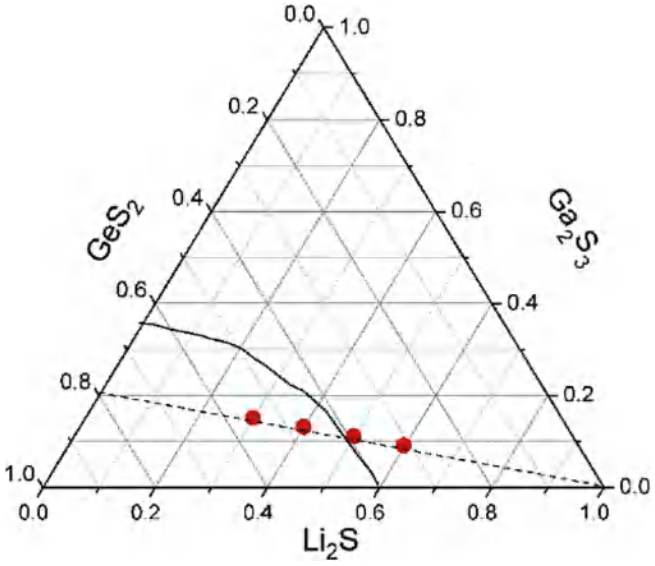

Fig. 2. Studied glass composition (red dots) with respect to the glass-forming region of the GeS_2-Ga_2S_3-Li_2S glass prepared by the melt-quench process (solid line) [15]. (For interpretation of the references to colour in this figure legend, the reader is referred to the Web version of this article.)

The amorphization process during mechanical milling was monitored by an X-ray diffractometer using Cu Kα radiation (D8 Advance, Bruker AXS GmbH, Germany). The cross-sectional morphology of the samples was characterized by a scanning electron microscope (Zeiss supra 55, Carl Zeiss GmbH, Germany). The Raman spectra were recorded by a Raman spectrometer (inVia, Renishaw Inc., UK) with a 532 nm diode-pumped solid-state laser as the source.

The ionic conductivity was measured using an ac impedance technique. The impedance spectra (10 Hz-1 MHz) were recorded in an Ar-filled glove box by a frequency response analyzer (Solartron 1260A, Solartron Analytical Inc., UK). To carry out the measurement, the as-prepared glass powders were cold-pressed into pellets under 330 MPa pressure (15 mm diameter and ~2 mm thickness). Both sides of the pellets were then coated with Au films as blocking electrodes. The conductivity of the samples was determined from the impedance spectra.

3. Results and discussion

3.1. Glass-forming ability

Fig. 1 shows the X-ray-diffraction (XRD) patterns of the glass powders in Series A. It can be seen that the increase of Li content results in a prolonged grinding duration in order to achieve a thorough amorphous state. For samples 3L4G1G and 4L4G1G, after 55 and 72 h grinding respectively, the diffraction peaks of crystalline phases disappear, indicating complete amorphization. However, for the samples 5L4G1G and 6L4G1G, even prolonged grinding duration cannot achieve complete amorphization. A serious caking occurs at the end stage of grinding which significantly reduces the grinding efficacy. The residual crystalline phase, which is different from the starting materials, does not agree well with any JCPDS cards. The indexing of the diffraction peaks reveals that the residual crystal is hexagonal, the lattice constants of which are a = 3.93 Å and c = 6.25 Å. It is suspected that the residual crystal might be a derivative of the hexagonal β-Ga_2S_3 (a = 3.682 Å, c = 6.031 Å) formed by the intercalation of Li. Therefore, the residual crystalline phase is a product of mechanical alloying.

To compare the amorphization ability of mechanical milling with that of the conventional melt-quench process, the composition of the samples in Series A is drawn in a pseudo ternary phase diagram along with the reported glass-forming region of the GeS_2-Ga_2S_3-Li_2S glass prepared by the melt-quench process (Fig. 2) [15]. The thoroughly amorphized samples 3L4G1G and 4L4G1G are within the glass-forming region, while the partially amorphized samples 5L4G1G and 6L4G1G are beyond the region. This indicates that mechanical milling with the parameters used in this study cannot evidently improve the glass-forming ability of the GeS_2-Ga_2S_3-Li_2S glasses.

To enhance the amorphization degree of sample 5L4G1G, whose composition is just beyond the glass-forming region, we partially substituted Li_2S by LiI in this composition [15], making the samples in Series B. The XRD patterns in Fig. 3 show that at the beginning of adding LiI, the glass-forming ability is improved so that a thorough amorphization can be achieved. After the LiI content exceeds 20 mol%, deterioration of the glass-forming ability occurs since the amorphization duration is prolonged. When the LiI content reaches 40 mol%, complete amorphization is no longer achievable. The residual crystal is confirmed to be cubic LiI (JCPDS Card No. 74-1974).

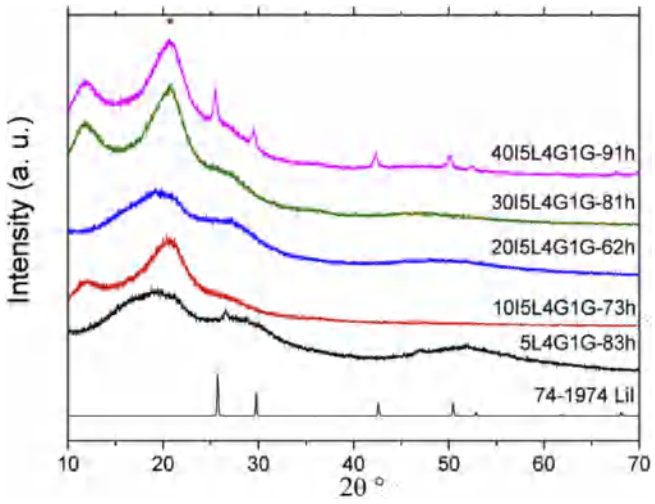

Fig. 3. XRD patterns of the GeS_2-Ga_2S_3-Li_2S-LiI glass powders in Series B, which are prepared by mechanical milling. Amorphization duration is noted in the legend.

3.2. Cross-sectional morphology

Scanning-electron-microscopy (SEM) images of the cross-section of the cold-pressed pellets are presented in Figs. 4 and 5. Fig. 4 shows the cross-sectional morphology of the samples in Series A. In the pellets made of the 3L4G1G and 4L4G1G glass powders, the sub-micrometer particles and a large number of voids can be clearly seen even though the pellets have been cold-pressed under 330 MPa. When the Li_2S content increases, the morphology shows remarkable change. Evident sintering between the particles appears in 5L4G1G. The particles are further sintered into bulk pieces in 6L4G1G. Such "room-temperature sintering" should also occur during ball milling, leading to serious caking and a poor grinding efficacy in these two samples as discussed above.

Fig. 5 shows the cross-sectional morphology of the samples in Series B. The substitution of Li_2S by LiI undoubtedly affects the "room-temperature sintering" phenomenon. At the beginning, the addition of LiI can reduce the sintering degree. As a result, large numbers of particles reappear in the pellet with 20 mol% LiI (20I5L4G1G). By adding more LiI, the "room-temperature sintering" occurs once again, as shown by the cross-section of 30I5L4G1G and 40I5L4G1G. It is worth noting that the variation of the sintering degree with the LiI content is in accordance with the ball-milling amorphization ability for the samples in Series B. In brief, the significant "room-temperature sintering" in Li-rich samples reduces the grinding efficacy, and consequently limits the glass-forming ability by mechanical milling.

3.3. Raman spectroscopy

To further verify the existence of glass network in the powders prepared by mechanical milling, Raman spectra were recorded as shown in Fig. 6. The Raman spectra can be divided into three regions which are normally observed in the Ge-Ga-S-based glasses prepared by the melt-quench method. The first region in the range 100–200 cm^{-1} contains the bands attributed to the symmetrical and asymmetrical bending of [GeS_4] tetrahedrons [19]. The second region in the range 200–300 cm^{-1} contains the bands attributed to the vibration of the homo-bond structural units [S_3Ge(Ga)-Ge(Ga)S_3] [20,21]. In the third region from 300 to 500 cm^{-1}, the most intense Raman signal appears, and is attributed to the vibration of [GeS_4] and [GaS_4] tetrahedrons with and without non-bridging sulfur (NBS) atoms [14,22]. The similarity of the Raman spectra of the ball-milled GeS_2-Ga_2S_3-Li_2S-LiI powders to the conventionally synthesized glasses indicates that they have similar glass network structure.

By examining the Raman spectra of the samples in Series A (Fig. 6 (a)), the structural evolution of the glass powders after the addition of Li_2S can be studied. With the increasing Li_2S content, the band attributed to 0-NBS [GeS_4] tetrahedrons (~350 cm^{-1}) decreases and broadens, while the band attributed to 2-NBS [GeS_4] tetrahedrons (~405 cm^{-1}) increases. Li_2S, acting as a network

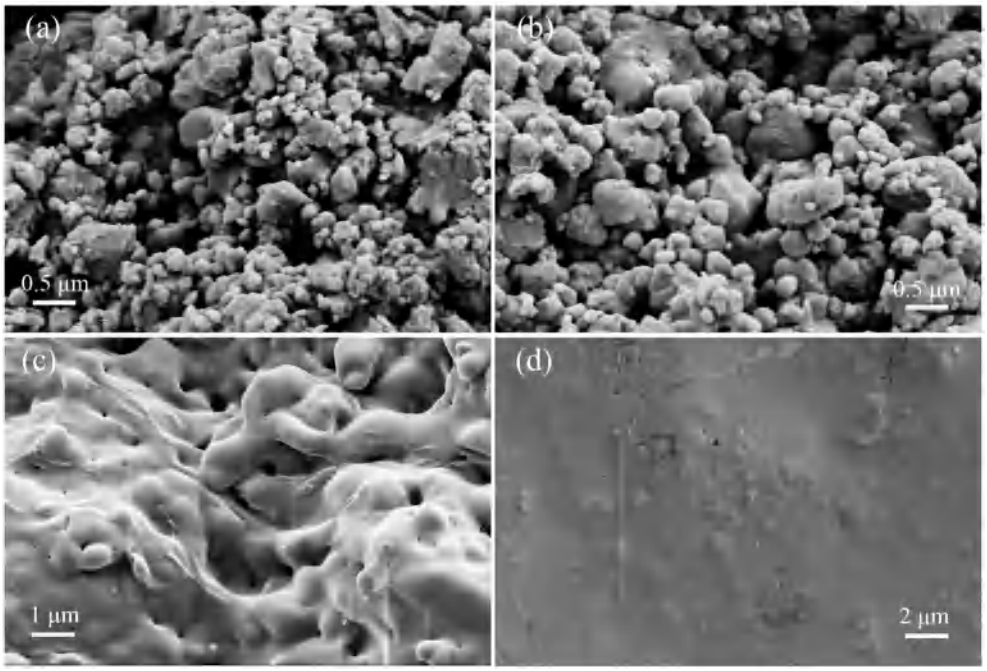

Fig. 4. SEM images showing the cross-section of the GeS_2-Ga_2S_3-Li_2S cold-pressed pellets (Series A). (a) 3L4G1G, (b) 4L4G1G, (c) 5L4G1G and (d) 6L4G1G.

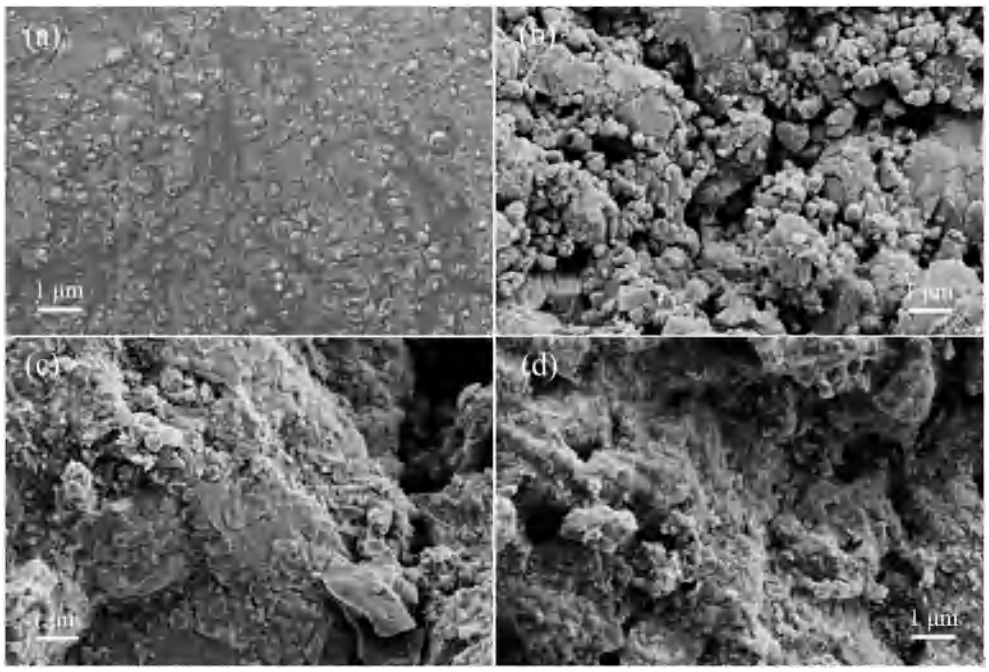

Fig. 5. SEM images showing the cross-section of the GeS_2-Ga_2S_3-Li_2S-LiI cold-pressed pellets (Series B). (a) 10I5L4G1G, (b) 20I5L4G1G, (c) 30I5L4G1G and (d) 40I5L4G1G.

modifier, introduces excess S^{2-} ions. The S^{2-} ions attack the bridging sulfur atoms that link the [GeS_4] or [GaS_4] tetrahedrons, disconnect the link, and convert bridging sulfur atoms into non-bridging sulfur atoms. The conversion of 0-NBS tetrahedrons to 2-NBS tetrahedrons results in the partial collapse of the three-dimensional (3D) glass network into one-dimensional one, as illustrated by Fig. 7. When the Li_2S content reaches 50 mol% (5L4G1G), the band attributed to 0-NBS tetrahedrons is so weak and broad that it integrates into the background signal. From this we infer that a significant collapse of the 3D glass network has occurred. When the Li_2S content reaches 60 mol% (6L4G1G), an additional peak appears at 370 cm^{-1}. This band is typically assigned to the symmetric stretching vibration of the two edge-shared [GeS_4] or [GaS_4] tetrahedrons [23]. From the sharp profile of this peak, we infer that it could be associated with the crystalline phase in this sample.

Fig. 6 (b) shows the Raman spectra of the samples in Series B. Different from the Raman spectra in Series A, the profile shows only a slight change in Series B, even though the highest substitution level of LiI has reached 40 mol%. This indicates that the influence of LiI on the Raman spectra is insignificant. Typically, the iodide plays the role of a glass network terminator, leading to the formation of [GeI_nS_{4-n}] ($n = 1$–3) tetrahedrons. The Raman signal of these tetrahedrons is between 200 and 250 cm^{-1} and is relatively weak [24]. Therefore, the addition of LiI does not evidently affect the main band between 250 and 500 cm^{-1}. This phenomenon is coincident with that observed in bulk glasses [19].

3.4. Ionic conductivity

The Nyquist plots of the complex impedance of the pellets cold-pressed from the as-milled powders are shown in Figs. 8 and 9. All the plots consist of a high-frequency arc and a low-frequency tail. The arc is attributed to the parallel of the geometrical capacitance and the resistance of the sample disk, while the tail, a typical signal of a Warburg element, is attributed to the diffusion of ions near the electrolyte/electrode interface [25]. The existence of the Warburg tail proves that all the samples are ionic conductive.

By fitting the Nyquist plots with an appropriate equivalent circuit [26], the room-temperature conductivity of the as-milled powders is deduced and listed in Table 1. In Series A, where the samples are composed of Ge_2S, Ga_2S_3 and Li_2S, the room temperature conductivity ranges from 10^{-6} S/cm to 10^{-5} S/cm, monotonically increasing with the Li content. In Series B, by partially substituting Li_2S by LiI, the room-temperature conductivity can be further improved. The highest conductivity in the completely amorphized samples, 3.18×10^{-4} S/cm, is achieved in 30I5L4G1G. The highest conductivity among the studied samples is 8.88×10^{-4} S/cm, observed in 40I5L4G1G which includes a small amount of LiI phase ($\sigma_{LiI@25^\circ C} \approx 10^{-7}$ S/cm).

To compare the ionic conductivity of the glass powders prepared by mechanical synthesis with that of bulk glasses, the room temperature conductivity of the bulk glasses with similar composition is summarized from the literature, as shown in Table 1. The typical room-temperature conductivity of the GeS_2-Ga_2S_3-Li_2S bulk glasses with similar composition (~50 mol% Li_2S) is ~10^{-5} S/cm [14,15]. By adding LiI to these bulk glasses, the room-temperature conductivity can reach a maximum of ~10^{-3} S/cm [15,22]. Thus, the conductivity of the bulk glass is only approximately 1–2 times higher than that of our mechano-synthesized powders. The lower conductivity of the powders than the bulk should be ascribed to the grain boundary resistance and the existence of voids between the particles (as shown in Figs. 4 and 5). The latter reduces the cross-section for ion conduction and therefore results in lower effective conductivity. Owing to the relatively low Young's modulus [27] and the "room-temperature sintering" phenomenon of sulfide glass powders as shown by the SEM images, the influence of the grain boundary on the ionic conductivity is minimized by simply cold-pressing the powders in our case, so that the conductivity of the pellets prepared by cold-pressing keeps the same order of magnitude with the bulk glasses. In brief, the practicality of the mechanical synthesis of the GeS_2-Ga_2S_3-Li_2S-LiI glasses does not adversely impact performance.

Fig. 10 shows the compositional dependence of the ionic

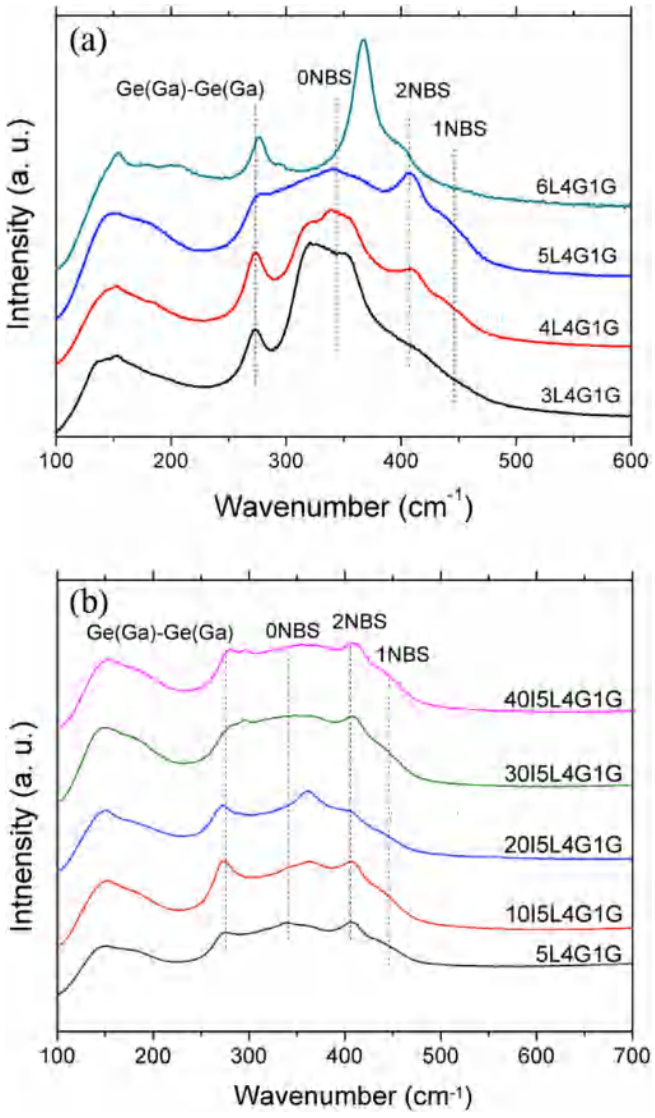

Fig. 6. Raman spectra of the glass powders in (a) Series A and (b) Series B. Major bands associated with 0-NBS, 1-NBS, 2-NBS [GeS_4] tetrahedrons, and Ge(Ga)-Ge(Ga) metallic homo-bonds are marked.

conductivity of the glass powders in Series A. The conductivity increases with increasing Li_2S content. It should be noted that the linearity between the conductivity and Li_2S content is not evident. Therefore, the increase of the conductivity is not mainly due to the increase of Li^+ concentration. A drastic increase of the conductivity occurs at 50 mol% Li_2S (5L4G1G), where the composition is just beyond the glass-forming region. It can be attributed to two facts. First, from the Raman results we infer that a significant collapse of the 3D glass network into one dimension occurs at 50 mol% Li_2S, and the network flexibility is improved, so that the Li^+ ions can more easily transport over the glass. A similar phenomenon has also been observed in the bulk glasses, composition of which is at the boundary of the glass-forming region [22]. Second, the SEM images in Fig. 4 illustrate that evident "room-temperature sintering" occurs in 5L4G1G and 6L4G1G. Consequently, the quantity of voids in these samples is significantly diminished, and the grain-boundary resistance is ameliorated in comparison with 3L4G1G and 4L4G1G.

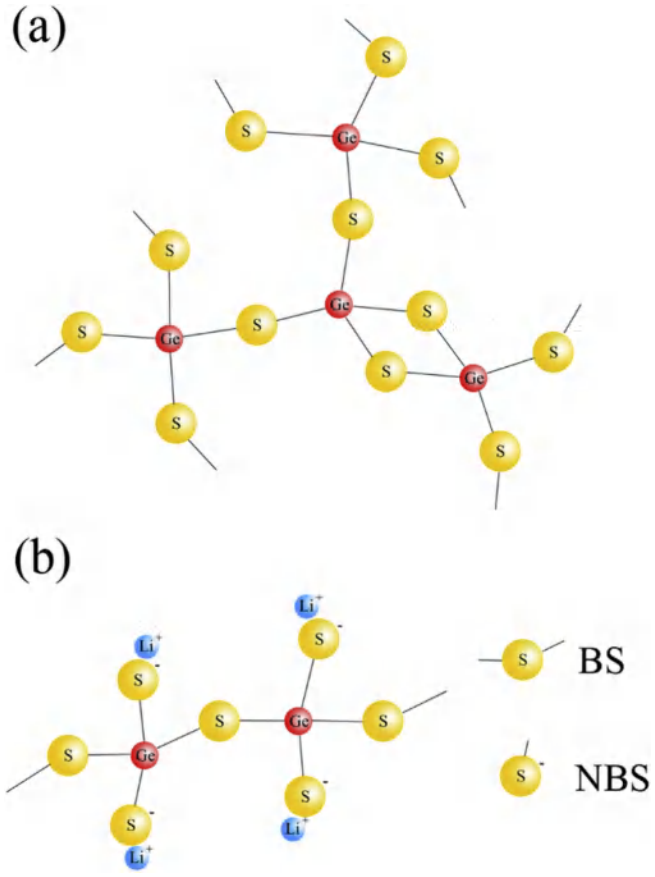

Fig. 7. Network units in the GeS_2-Ga_2S_3-Li_2S glass. (a) [GeS_4] tetrahedrons without non-bridging sulfur atoms (0-NBS) forming a 3D glass network; (b) [GeS_4] tetrahedrons with two non-bridging sulfur atoms (2-NBS) leading to a partial collapse of the network into one dimension.

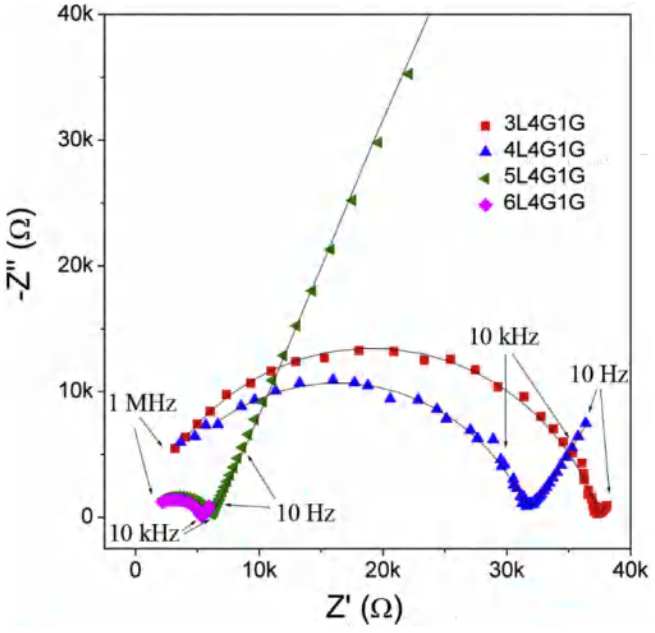

Fig. 8. Room-temperature impedance spectra of the GeS_2-Ga_2S_3-Li_2S cold-pressed pellets in Series A. Thin solid lines present the fitting results by an equivalent circuit.

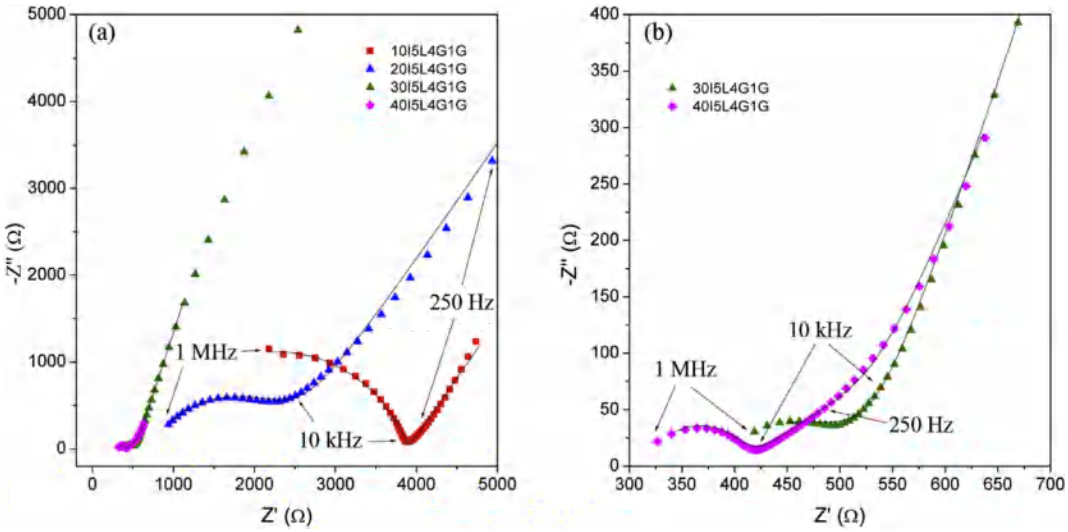

Fig. 9. Room-temperature impedance spectra of the GeS_2-Ga_2S_3-Li_2S-LiI cold-pressed pellets in Series B. (b) is the magnified high-frequency part of (a).

Table 1
Room temperature conductivity σ of the glass powders prepared by mechanical milling, in comparison with that of the bulk glasses reported in the literature (in italics).

LiI (mol%)	Li_2S (mol%)	GeS_2 (mol%)	Ga_2S_3 (mol%)	σ (S/cm)	Sample/Ref.
0	30	56	14	1.28×10^{-6}	3L4G1G
0	40	48	12	1.89×10^{-6}	4L4G1G
0	50	40	10	7.76×10^{-6}	5L4G1G
0	60	32	8	1.044×10^{-5}	6L4G1G
0	*45*	*45*	*10*	*9.37×10^{-6}*	*Ref. [15], bulk glass*
0	*50*	*45*	*5*	*2.27×10^{-5}*	*Ref. [15], bulk glass*
0	*46*	*46*	*8*	*1.58×10^{-6}*	*Ref. [14], bulk glass*
0	*53*	*40*	*7*	*6.31×10^{-6}*	*Ref. [14], bulk glass*
10	45	36	9	1.40×10^{-5}	10I5L4G1G
20	40	32	8	3.50×10^{-5}	20I5L4G1G
30	35	28	7	3.18×10^{-4}	30I5L4G1G
40	30	24	6	8.88×10^{-4}	40I5L4G1G
30	*31.5*	*31.5*	*8*	*9.16×10^{-4}*	*Ref. [15], bulk glass*
40	*27*	*27*	*6*	*10.4×10^{-4}*	*Ref. [15], bulk glass*

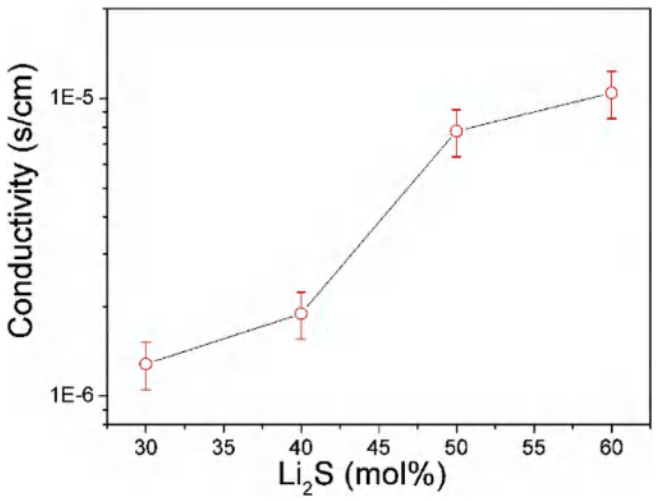

Fig. 10. Composition dependence of ionic conductivity of the GeS_2-Ga_2S_3-Li_2S glass powders in Series A.

4. Conclusions

Ionic conductive GeS_2-Ga_2S_3-Li_2S-LiI glass powders were mechanically synthesized by ball milling. The room-temperature ionic conductivity of the GeS_2-Ga_2S_3-Li_2S powders ranges from 10^{-6} to 10^{-5} S/cm with the increase of Li_2S content from 30 to 60 mol%. By partially substituting Li_2S by LiI, the conductivity can be further improved and reaches 3.18×10^{-4} S/cm in the completely amorphized sample with 30 mol% LiI (30I5L4G1G), and 8.88×10^{-4} S/cm in the sample with 40 mol% LiI (40I5L4G1G), which includes a small amount of LiI phase. The conductivity of the powders studied in this paper, which is simply measured from the cold-pressed samples, is comparable with that of the bulk glasses reported in the literature. Although mechanical synthesis cannot evidently improve the glass-forming ability of the GeS_2-Ga_2S_3-Li_2S-LiI system, this technique can eliminate the quartz glass reaction container, and therefore reduces the production cost. Mechanical synthesis is more suitable for the large-scale production of GeS_2-Ga_2S_3-Li_2S-LiI solid-state electrolyte.

This work also reveals the "room-temperature sintering" phenomenon in Li-rich GeS_2-Ga_2S_3-Li_2S-LiI glass powders. Such a phenomenon has two-sided effect: It causes serious caking during ball milling and therefore limits the efficiency of mechanical synthesis, while reducing the grain-boundary resistance so that high ionic conductivity can be achieved by cold-pressing.

Acknowledgements

This work was the financially supported by the National Natural Science Foundation of China (Grant No. 61504085/51702216), the Natural Science Foundation of Guangdong Province (Grant No. 2017A030313325), the Shenzhen Science and Technology Foundation (Grant No. JCYJ20140509172719312), and the Natural Science Foundation of Shenzhen University (Grant No. 827-000037/201520).

References

[1] X. Judez, H. Zhang, C. Li, G.G. Eshetu, J.A. González-Marcos, M. Armand, L.M. Rodriguez-Martinez, Review—solid electrolytes for safe and high energy density lithium-sulfur batteries: promises and challenges, J. Electrochem. Soc. 165 (2018) A6008–A6016.
[2] A. Manthiram, X. Yu, S. Wang, Lithium battery chemistries enabled by solid-state electrolytes, Nat. Rev. Microbiol. 2 (2017) 16103.

[3] Z. Lin, C. Liang, Lithium-sulfur batteries: from liquid to solid cells, J. Mater. Chem. A 3 (2015) 936–958.
[4] C. Li, H. Zhang, L. Otaegui, G. Singh, M. Armand, L.M. Rodriguez-Martinez, Estimation of energy density of Li-S batteries with liquid and solid electrolytes, J. Power Sources 326 (2016) 1–5.
[5] Y. Kato, S. Hori, T. Saito, K. Suzuki, M. Hirayama, A. Mitsui, M. Yonemura, H. Iba, R. Kanno, High-power all-solid-state batteries using sulfide superionic conductors, Nat. Energy 1 (2016) 16030.
[6] Y. Seino, T. Ota, K. Takada, A. Hayashi, M. Tatsumisago, A sulphide lithium super ion conductor is superior to liquid ion conductors for use in rechargeable batteries, Energy Environ. Sci. 7 (2014) 627–631.
[7] N. Kamaya, K. Homma, Y. Yamakawa, M. Hirayama, R. Kanno, M. Yonemura, T. Kamiyama, Y. Kato, S. Hama, K. Kawamoto, A. Mitsui, A lithium superionic conductor, Nat. Mater. 10 (2011) 682–686.
[8] H.U. Choi, J.S. Jin, J.-Y. Park, H.-T. Lim, Performance improvement of all-solid-state Li-S batteries with optimizing morphology and structure of sulfur composite electrode, J. Alloy Compd. 723 (2017) 787–794.
[9] F. Han, J. Yue, X. Fan, T. Gao, C. Luo, Z. Ma, L. Suo, C. Wang, High-performance all-solid-state lithium–sulfur battery enabled by a mixed-conductive Li_2S nanocomposite, Nano Lett. 16 (2016) 4521–4527.
[10] R. Xu, Z. Wu, S. Zhang, X. Wang, Y. Xia, X. Xia, X. Huang, J. Tu, Construction of all-solid-state batteries based on a sulfur-graphene composite and $Li_{9.54}Si_{1.74}P_{1.44}S_{11.7}Cl_{0.3}$ solid electrolyte, Chem. Eur J. 23 (2017) 13950–13956.
[11] Z. Lin, Z. Liu, W. Fu, N.J. Dudney, C. Liang, Lithium polysulfidophosphates: a family of lithium-conducting sulfur-rich compounds for lithium–sulfur batteries, Angew. Chem. Int. Ed. 52 (2013) 7460–7463.
[12] X. Yao, N. Huang, F. Han, Q. Zhang, H. Wan, J.P. Mwizerwa, C. Wang, X. Xu, High-performance all-solid-state lithium–sulfur batteries enabled by amorphous sulfur-coated reduced graphene oxide cathodes, Adv. Eng. Mater. 7 (2017), 1602923.
[13] S. Cozic, A. Bréhault, D.L. Coq, T. Usuki, GeS_2–Ga_2S_3–LiCl glass system: electrical conductivity and structural considerations, Int. J. Appl. Glass Sci. 7 (2016) 513–523.
[14] M. Yamashita, H. Yamanaka, Formation and ionic conductivity of Li_2S–GeS_2–Ga_2S_3 glasses and thin films, Solid State Ionics 158 (2003) 151–156.
[15] J. Saienga, Y. Kim, B. Campbell, S.W. Martin, Preparation and characterization of glasses in the LiI+Li_2S+GeS_2+Ga_2S_3 system, Solid State Ionics 176 (2005) 1229–1236.
[16] B. Xue, L. Calvez, M. Allix, G. Delaizir, X.-H. Zhang, Amorphization by mechanical milling for making IR transparent glass-ceramics, J. Am. Ceram. Soc. 99 (2016) 1573–1578.
[17] M. Hubert, E. Petracovschi, X.-H. Zhang, L. Calvez, Synthesis of germanium–gallium–tellurium (Ge–Ga–Te) ceramics by ball-milling and sintering, J. Am. Ceram. Soc. 96 (2013) 1444–1449.
[18] M. Hubert, G. Delaizir, J. Monnier, C. Godart, H.-L. Ma, X.-H. Zhang, L. Calvez, An innovative approach to develop highly performant chalcogenide glasses and glass-ceramics transparent in the infrared range, Optic Express 19 (2011) 23513–23522.
[19] J. Kolář, T. Wágner, V. Zima, Š. Stehlík, B. Frumarová, L. Beneš, M. Vlček, M. Frumar, S.O. Kasap, Ion conductive chalcohalide glasses in LiI–Ga_2S_3–GeS_2 system, J. Non-Cryst. Solids 357 (2011) 2223–2227.
[20] I. Pethes, V. Nazabal, R. Chahal, B. Bureau, I. Kaban, S. Belin, P. Jóvári, Local motifs in GeS_2–Ga_2S_3 glasses, J. Alloy Compd. 673 (2016) 149–157.
[21] T. Haizheng, Z. Xiujian, J. Chengbin, Raman spectroscopic study on the microstructure of GeS_2–Ga_2S_3–KCl glasses, J. Mol. Struct. 697 (2004) 23–27.
[22] J. Saienga, S.W. Martin, The comparative structure, properties, and ionic conductivity of LiI + Li_2S + GeS_2 glasses doped with Ga_2S_3 and La_2S_3, J. Non-Cryst. Solids 354 (2008) 1475–1486.
[23] H. Guo, H. Tao, Y. Zhai, S. Mao, X. Zhao, Raman spectroscopic analysis of GeS_2–Ga_2S_3–PbI_2 chalcohalide glasses, Spectrochim. Acta, Part A 67 (2007) 1351–1356.
[24] J. Ren, Q. Yan, T. Wagner, V. Zima, M. Frumar, B. Frumarova, G. Chen, Conductivity study on GeS_2-Ga_2S_3-AgI-Ag chalcohalide glasses, J. Appl. Phys. 114 (2013), 023701.
[25] E. Barsoukov, J.R. Macdonald, Impedance Spectroscopy: Theory, Experiment, and Applications, second ed., John Wiley & Sons, Inc., Hoboken, NJ, USA, 2005.
[26] B.J. Neudecker, W. Weppner, Li_9SiAlO_8: a lithium ion electrolyte for voltages above 5.4 V, J. Electrochem. Soc. 143 (1996) 2198–2203.
[27] A. Sakuda, A. Hayashi, Y. Takigawa, K. Higashi, M. Tatsumisago, Evaluation of elastic modulus of Li_2S-P_2S_5 glassy solid electrolyte by ultrasonic sound velocity measurement and compression test, J. Ceram. Soc. Jpn. 121 (2013) 946–949.